PROCEEDINGS OF SCIENCE

Double synchrotron self-absorption spectrum of the blazar 3C 454.3 and its B-field strength

Hyeon-Woo Jeong[a,b,*] **and Sang-Sung Lee**[a,b]

[a] *Astronomy and Space Science, University of Science and Technology 34113, Daejeon, Republic of Korea*

[b] *Korea Astronomy and Space Science Institute, 34055, Daejeon, Republic of Korea*

E-mail: hwjeong@kasi.re.kr, sslee@kasi.re.kr

The blazar 3C 454.3 is known for its strong outburst across the whole electromagnetic spectrum. Multi-wavelength radio observations enable us to study the spectral variability of relativistic radio jet in the source. In this work, we use multi-wavelength radio observations at 3 GHz to 340 GHz. From the spectral analysis using the multi-wavelength data, we found two synchrotron self-absorption (SSA) features in the source spectra for compact variable emission regions. One peak of the SSA spectral features is found at a frequency range of 3–37 GHz (LSS), and the other at 55–125 GHz (HSS). By using the derived SSA turnover frequency and peak flux density, we estimated B-field strength ($B_{\rm SSA}$) for the SSA regions in the relativistic jet. The estimated B-field strengths of the HSS and the LSS features are $\gtrsim$ 0.1 mG and $>$ 3 mG, respectively. The LSS B-field strength is comparable at the first epoch, and even stronger than the estimated B-field strength ($B_{\rm EQ}$ = 2 $\sim$ 5 mG) under the equipartition condition in the other epochs before the 2014 June γ-ray flare, implying a magnetic dominance in this region. We found the LSS region is related to the quasi-stationary component (C) $\sim$ 0.6 mas away from the VLBI core at 43 GHz. And we found that component C is considered as a recollimation shock based on the analysis of the jet width and polarimetric characteristics.

15th European VLBI Network Mini-Symposium and Users' Meeting (EVN2022)
11-15 July 2022
University College Cork, Ireland

*Speaker

PoS(EVN2022)008

1. Introduction

Blazar is a subclass of AGNs, whose jet is closely aligned toward us. The blazar 3C 454.3 is one of the most bright astronomical objects in the sky. The source has shown many flaring activities in γ-ray (e.g., [3, 4, 8, 14, 19]). In radio wavelengths, the observed emission is radiated by accelerated charged particles gyrating magnetic (B) field lines ([16, 20]). B-fields are believed to be in charge of launching, accelerating, and collimating jets in AGNs. Therefore, investigating B-field environments in jets is important for understanding jet physics.

The source was in an active state in 2014 June and was monitored with many telescopes with wide frequency coverage (3–340 GHz, [2, 5, 6, 17]). These observations give us a great opportunity for analysing the spectra of the jet.

2. Observations

Single-dish data were collected from monitoring programs, such as the Fermi-GST AGN Multi-frequency Monitoring Alliance (F-GAMMA, [5]) at a frequency range of 3–43 GHz, the Owens Valley Radio Observatory (OVRO, [18]) at 15 GHz and the MOnitoring of GAmma-ray Bright AGNs (MOGABA, [11]), using the Korean VLBI Network (KVN) 21 m telescope at 22 and 43 GHz. High-frequency data were obtained from interferometric array monitoring programs, such as the Monitoring of γ-ray AGN with Radio, Millimeter, and Optical Telescopes (MARMOT, [17]) at 95 GHz, the Submillimeter Array (SMA, [6]) at 230 GHz and the Atacama Large Millimeter/submillimeter Array (ALMA) at 91, 103, 233 and 337 GHz.

In addition to the single-dish and array observational data, we included VLBI data from the observations using European VLBI Network (EVN) at 5 GHz and from two Very Long Baseline Array monitoring programs (VLBA) at 15 GHz (Monitoring of Jets in Active galactic nuclei with VLBA Experiments, MOJAVE, [12]) and at 43 GHz (VLBA-BU-BLAZAR, [9]).

3. Results and Discussion

The multi-wavelength flux measurements enabled us to see two synchrotron self-absorption (SSA) peaks in the source spectra after decomposing a quiescent spectrum of the source: one at lower turnover frequencies ($\nu_{\rm m}$) 3−37 GHz (LSS), and the other at higher frequencies, 55−125 GHz (HSS), as shown in Figure 1. The obtained variable spectra were fitted with an SSA model ([21]).

Figure 2 shows flux density variation of the SSA spectra at 5 and 43 GHz with VLBI measurements. At 43 GHz, the HSS fluxes closely follow the 43 GHz core flux variation. Thus, the remaining emission from the extended jet structure is corresponding to the LSS emission. We found that the flux variability trend of the LSS at 5 GHz is similar to that of the 5 GHz radio core.

Spectral analyses on the quasi-stationary component (C, $\sim$ 0.6 mas away from the core) were performed with the VLBA observations at 15, 22, and 43 GHz (Figure 3). Component C shows the optically thin spectrum in 2013 May, however, a turnover frequency of around 22 GHz in 2016, implying that component C is another SSA emitting region.

B-field strength in the jet can be measured using the derived SSA parameters ($B_{\rm SSA}$, [13]) and using the equipartition relations from [15] ($B_{\rm EQ}$, [10]), as shown in Figure 4. The SSA parameters

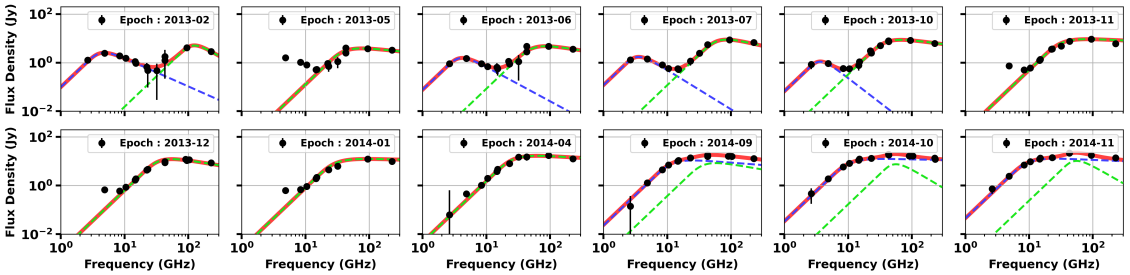

Figure 1: Source spectra with double SSA components after decomposing a quiescent spectrum. Green (HSS) and blue (LSS) dashed lines are individual SSA spectra. The red solid line indicates the sum of the two SSA spectra. Black dots are the observed data.

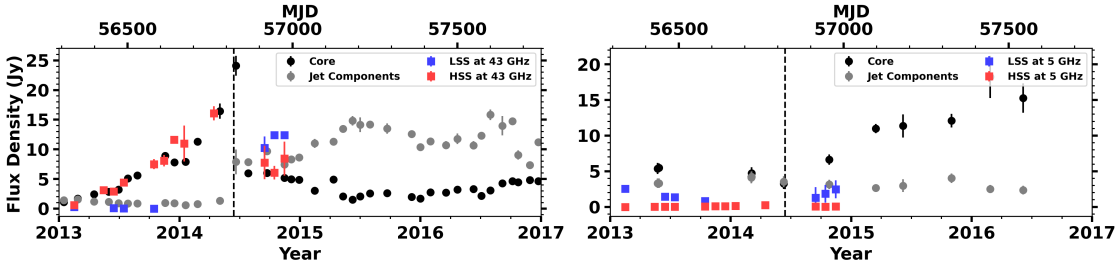

Figure 2: Variability of the observed flux density of the VLBI components and inferred flux density from the SSA models at 43 GHz (*Left*) and 5 GHz (*Right*). Red and blue squares are the HSS- and LSS-inferred flux density, respectively. The black dots are the observed flux density of the core. The gray dots are the sum of the observed flux density of the remaining jet components

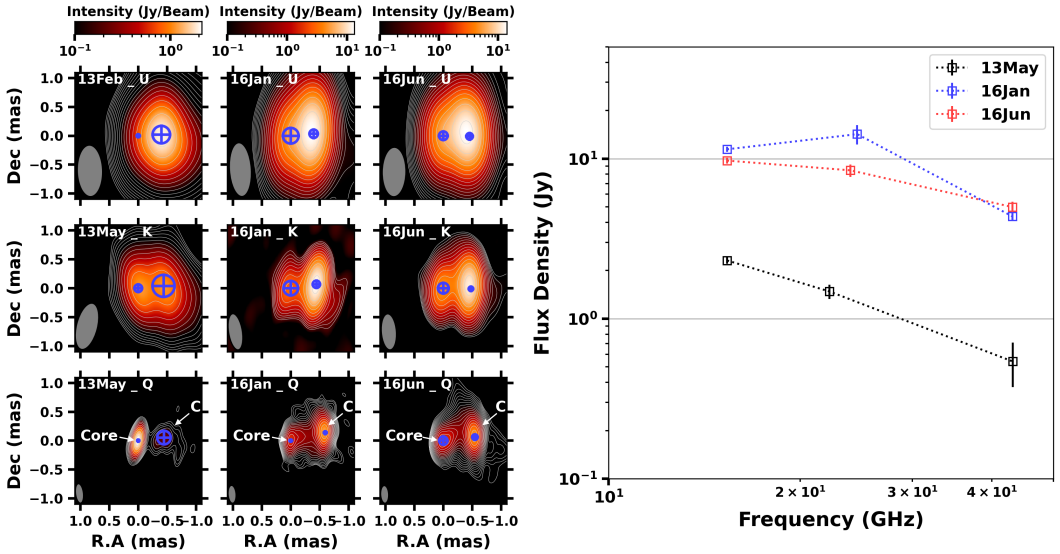

Figure 3: *Left*: The VLBA maps in 2013 and 2016 at 15, 22, and 43 GHz (from top to bottom). Modeled core and component C is denoted as a blue circle with a plus sign. Color maps and contours indicate source intensity. *Right*: The obtained spectrum of the component C.

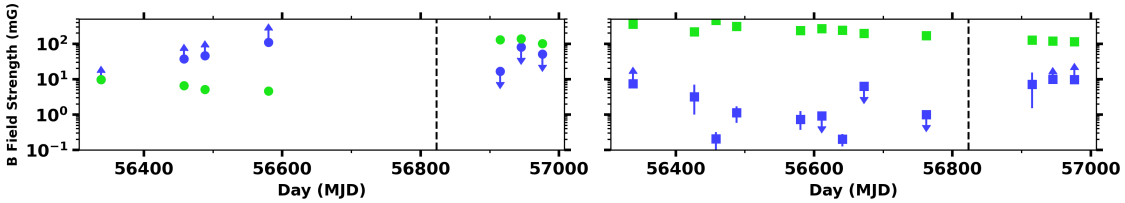

Figure 4: Time variation of B-field strength for both the LSS (*Left*) and the HSS (*Right*) emission regions. Blue and green dots indicate estimated $B_{\rm SSA}$ and $B_{\rm EQ}$ in units of mG, respectively. Vertical black dashed lines indicate 2014-06-14. The up and down arrows indicate lower and upper limits, respectively.

Table 1: The estimated B-Field strength and the observed brightness temperature. The upper and lower uncertainties are propagated individually through the standard error propagation model using the SSA parameters.

Epoch (Year – Month)	$B_{\rm SSA,LSS}$ (mG)	$B_{\rm EQ,LSS}$ (mG)	$T_{\rm b,obs,LSS}$ (10^{11} K)	$B_{\rm SSA,HSS}$ (mG)	$B_{\rm EQ,HSS}$ (mG)	$T_{\rm b,obs,HSS}$ (10^{11} K)
2013 – 02	> 9.69	$9.75^{+1.03}_{-1.03}$	1.63 ± 0.36	> 7.50	$355.16^{+56.66}_{-50.20}$	7.98 ± 2.36
2013 – 05	–	–	-	$3.19^{+3.89}_{-2.19}$	$215.71^{+21.52}_{-20.54}$	6.92 ± 2.06
2013 – 06	> 37.39	$6.61^{+0.78}_{-0.78}$	0.78 ± 0.19	$0.21^{+0.12}_{-0.11}$	$462.04^{+43.84}_{-43.75}$	34.04 ± 5.85
2013 – 07	> 46.38	$5.10^{+0.74}_{-0.74}$	0.64 ± 0.17	$1.13^{+0.60}_{-0.54}$	$308.77^{+30.20}_{-30.14}$	16.19 ± 2.75
2013 – 10	> 110.09	$4.62^{+0.71}_{-0.68}$	0.42 ± 0.15	$0.73^{+0.53}_{-0.36}$	$234.38^{+18.42}_{-17.93}$	14.85 ± 2.75
2013 – 11	–	–	-	< 0.93	$267.94^{+26.41}_{-25.16}$	12.81 ± 3.90
2013 – 12	–	–	-	$0.20^{+0.08}_{-0.08}$	$240.44^{+22.38}_{-22.38}$	27.80 ± 4.88
2014 – 01	–	–	-	< 6.31	$196.65^{+33.45}_{-28.30}$	5.21 ± 4.19
2014 – 04	–	–	-	< 1.01	$170.30^{+20.01}_{-19.73}$	10.62 ± 3.07
2014 – 09	< 16.71	$129.13^{+14.48}_{-14.56}$	21.67 ± 10.64	$7.10^{+8.31}_{-5.58}$	$126.59^{+18.60}_{-12.46}$	4.95 ± 1.61
2014 – 10	< 80.46	$138.97^{+10.90}_{-10.74}$	11.80 ± 3.27	> 9.97	$119.72^{+8.93}_{-8.77}$	4.64 ± 0.63
2014 – 11	< 50.85	$101.09^{+9.42}_{-9.51}$	12.51 ± 2.97	> 9.69	$114.35^{+11.43}_{-11.28}$	4.70 ± 1.24

can also be used to calculate the observed brightness temperature. The Doppler factor of the LSS, $\delta_{\rm LSS} = 20.3 \pm 1.8$, is obtained from the downstream (e.g., more than 0.4 mas away from the core) jet components observed by the 43 GHz monitoring program ([7, 9, 22]). Using $\delta_{\rm LSS}$, we found that the intrinsic brightness temperature of the LSS is lower ($(4 - 15) \times 10^9$ K) than the equipartition brightness temperature ($T_{\rm EQ} = 5 \times 10^{10}$ K). The estimated magnetic field strength and the intrinsic brightness temperature (Table 1), indicate that the LSS emitting region was magnetically dominated before the γ-ray flare.

Figure 5 shows the stacked map of the VLBA 43 GHz data in the period of 2013 January–2016 December. The stacked map was used for finding jet ridgeline (i.e., the flow of jet plasma) and for investigating time-averaged linear polarimetric characteristics. Along the ridgeline, a decrease of jet width (from $\sim 10^4\ r_{\rm g}$ to $\sim 8.7 \times 10^3\ r_{\rm g}$, $r_{\rm g}$: gravitational radius) was found at $\sim 7 \times 10^5\ r_{\rm g}$. Additionally, both polarized intensity and degree of polarization are higher at the component

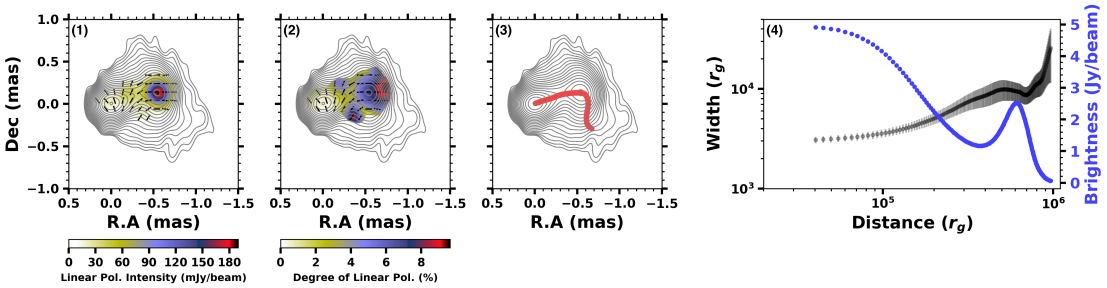

Figure 5: The first three panels are stacked (2013 Jan – 2016 Dec) maps with contours of the Stokes *I* map. Color maps are (1): Linear polarized intensity, (2): Degree of linear polarization. The black ticks in the first two panels are EVPAs. In panel (3), the red circles represent the jet ridgeline. In the panel, (4), black error bars, and blue dots are the estimated jet width and brightness along the ridgeline, respectively.

C (> 180 mJy, ∼ 8%) than the radio core (< 30 mJy, ∼ 1%). The electric vector position angles (EVPAs) are parallel with the ridgeline at component C.

In this work, we found a decrease in jet width, magnetic dominance, and high both polarized intensity and degree of polarization in component C. These characteristics may indicate a possible recollimation shock in component C.

4. Conclusions

3C 454.3 showed two SSA peaks in the spectra, LSS and HSS, and the estimated B-field strength and the intrinsic brightness temperature in the LSS indicate that the LSS emitting region was magnetically dominated in 2013. In addition to that, we found a jet width decrease, higher polarized intensity (and degree of polarization), and parallel EVPA in component C. These may indicate that component C is likely to be a recollimation shock.

Acknowledgments

This research has made use of data from the OVRO 40-m monitoring program [18], supported by private funding from the California Insitute of Technology and the Max Planck Institute for Radio Astronomy, and by NASA grants NNX08AW31G, NNX11A043G, and NNX14AQ89G and NSF grants AST-0808050 and AST- 1109911. This paper has used data from the MARMOT program that was a key-science program running at CARMA. The data from this program are provided by Dr. Talvikki Hovatta. The Submillimeter Array is a joint project between the Smithsonian Astrophysical Observatory and the Academia Sinica Institute of Astronomy and Astrophysics and is funded by the Smithsonian Institution and the Academia Sinica. This paper makes use of the following ALMA data: ADS/JAO.ALMA#2011.0.01234.S. ALMA is a partnership of ESO (representing its member states), NSF (USA) and NINS (Japan), together with NRC (Canada), MOST and ASIAA (Taiwan), and KASI (Republic of Korea), in cooperation with the Republic of Chile. The Joint ALMA Observatory is operated by ESO, AUI/NRAO and NAOJ. This research has made use of data from the MOJAVE database that is maintained by the MOJAVE team [12]). This study makes use of VLBA data from the VLBA-BU Blazar Monitoring Program (BEAM-ME and

VLBA-BU-BLAZAR; http://www.bu.edu/blazars/BEAM-ME.html), funded by NASA through the Fermi Guest Investigator Program. The VLBA is an instrument of the National Radio Astronomy Observatory. The National Radio Astronomy Observatory is a facility of the National Science Foundation operated by Associated Universities, Inc.

References

[1] Algaba J.-C et al., 2018, ApJ, 859, 128

[2] Angelakis E et al., 2019, A&A, 626, A60

[3] Bulgarelli A et al., 2014, ATel, 6234

[4] Escande L., Tanaka Y. T., 2009, ATel, 2328

[5] Fuhrmann L et al., 2016, A&A, 596, A45

[6] Gurwell M. A et al., 2007, ASPC, 375, 234

[7] Jorstad S. G et al., 2005, AJ, 130, 1418

[8] Jorstad S et al., 2015, ATel, 7942

[9] Jorstad S. G et al., 2017, ApJ, 846, 98

[10] Kataoka J et al., 2005, ApJ, 622, 797

[11] Lee S.-S et al., 2013, EPJWC, 61, 07007

[12] Lister M. L et al., 2018, ApJS, 234, 12

[13] Marscher A. P., 1983, ApJ, 264, 296

[14] Munar-Adrover P et al., 2016, ATel, 9186

[15] O'Dea C. P., Owen F. N., 1987, ApJ, 316, 95

[16] Pacholczyk A. G., 1970, ranp.book

[17] Ramakrishnan V et al., 2016, MNRAS, 456, 171

[18] Richards J. L et al., 2011, ApJS, 194, 29

[19] Sanchez D., Escande L., 2010, ATel, 3041

[20] Schwinger J., 1949, PhRv, 75, 1912

[21] Türler M et al., 1999, A&AS, 134, 89

[22] Weaver Z. R et al., 2022, ApJS, 260, 12